Journal of Sound and Vibration (1999) **224**(3), 541–561
Article No. jsvi.1999.2197, available online at http://www.idealibrary.com on IDEAL®

DYNAMICS OF MULTI-SPAN CONTINUOUS STRAIGHT BRIDGES SUBJECT TO MULTI-DEGREES OF FREEDOM MOVING VEHICLE EXCITATION

S. MARCHESIELLO, A. FASANA,
L. GARIBALDI AND B.A.D. PIOMBO

Dipartimento di Meccanica, Politecnico di Torino, Corso Duca degli Abruzzi, 24
I-10129 *Torino, Italy*

(*Received* 19 *September* 1997, *and in final form* 1 *February* 1999)

The paper presents an analytical approach to the problem of vehicle–bridge dynamic interaction. Starting from early studies based on a simply supported beam interacting with a lumped mass moving at constant speed, in recent years researchers have improved the models of both the bridge and the vehicle. On this basis, the bridge is modelled here as a multi-span continuous isotropic plate; its response to external loads is defined by applying the mode superposition principle and takes into account both flexural and torsional mode shapes, the latter being usually neglected in the literature. The plate is considered proportionally damped and its modes are computed by means of the Rayleigh–Ritz method. The scheme adopted for the vehicle consists of a seven degrees-of-freedom system moving at constant speed over the isotropic rough bridge surface. The numerical investigation, based on these analytical models, refers to a three-span bridge and includes the importance of torsional mode shapes, of road surface irregularities and of vehicle speed.

1. INTRODUCTION

The problem of vehicle-bridge interaction has been the subject of study for many researchers during the last few years. A number of different approaches can be found throughout the literature, most of them attempting to improve the analytical model of the physical interaction between the bridge and the vehicles moving over it.

The problem has become more interesting with bridge structures getting gradually lighter and more flexible, while the speed and the weight of moving loads have grown conversely.

Early models adopted to simulate bridge–vehicle interaction normally considered simply supported beams with a single, lumped load moving at constant speed along its span. These models mainly evolve from the original work by Timoshenko et al. [1] and Fryba [2].

0022-460X/99/280541 + 21 $30.00/0

This simple case has been studied by using different mathematical approaches, i.e. by using the Euler–Bernoulli beam [3,4], or the Timoshenko representation of the beam with moving loads [5].

Some improvements have been made by the adoption of more refined models of the moving load, namely a spring-dashpot single-degree-of-freedom (s.d.o.f) vehicle [6], or multi-degrees-of-freedom (m.d.o.f) systems with separated body and wheel masses [2, 7–10]; their speed has sometimes been considered non-constant [11, 12]; the road surface, considered smooth in many papers, has also been introduced in the models by using random distribution of roughness [6, 8–10]; the main drawback of the above-mentioned models is their inability to calculate the effects of torsional shapes of the bridge deck, thus introducing a severe approximation with respect to the real structure.

By replacing the beams with an isotropic plate to represent the deck behaviour, a consistent step forward has been taken. With regard to this, vast literature can be found concerning the modal behaviour of plates with different boundary conditions: for at least two simply supported opposite edges, the Lévy-type solution reported by Leissa [13], Sakata [14] and Gorman [15] can be adopted, while for all other boundary conditions, different solution methods can be found, as in the classic work by Gorman [15], or by using the well-known Rayleigh–Ritz solution [13, 16–25] or, also, by using the Kantorovich method [20, 26]. With respect to the Rayleigh–Ritz approach, different choices allowed for the admissible functions should be mentioned: characteristic beam functions [13, 21, 23], two-dimensional plate functions [17, 25] or orthogonal polynomial functions [16, 18–20, 22, 24].

This paper deals with the interaction of multi-span continuous bridges modelled by isotropic plates with m.d.o.f. vehicles moving at constant speed. The surface considered as the interface between the vehicle and the bridge can be smooth or rough. The same kind of problem has already been faced by other authors by using FE simulations for the bridge deck [27] or by considering planar vehicle models [28].

In this paper, the modal superposition of analytical deflections, together with a modal decomposition of the forces acting on the bridge, is adopted and the vehicle–bridge interaction is computed iteratively. In principle, the vehicle can be modelled in many ways: the one used throughout the paper has seven d.o.f. including pitch, roll and heave motions.

Some simulations are reported, showing the contribution of torsional modes on the overall displacement at the mid-span; the importance of surface roughness and vehicle speed are also pointed out; the amplification factor, often reported as a function of the span length [9], is presented here with respect to the vehicle speed as in references [6, 27].

2. DYNAMIC RESPONSE OF BRIDGES TO VEHICLE LOADS

2.1. EQUATION OF MOTION AND MODAL SUPERPOSITION

The dynamic behaviour of multi-span continuous bridges is governed by the equation [29]

$$\bar{m}(\mathbf{x})\frac{\partial^2 w}{\partial t^2}(\mathbf{x},t) + C\left\{\frac{\partial w}{\partial t}(\mathbf{x},t)\right\} + L\{w(\mathbf{x},t)\} = f(\mathbf{x},t), \tag{1}$$

where $\mathbf{x}$ is a two-dimensional position vector, t is the time, $\bar{m}(\mathbf{x})$ is the distributed mass per unit area, $w(\mathbf{x}, t)$ is the transverse deflection of the bridge, measured upwards from its equilibrium position, L is a differential stiffness operator with respect to spatial variables, C is a viscous damping operator with respect to spatial variables and $f(\mathbf{x}, t)$ is the force transmitted by the vehicle onto the bridge.

The general formulation of the equation of motion is based on the following assumptions: the structure has a linear elastic behaviour with small deflections and viscous damping, and the effects of shear deformation and rotary inertia are neglected.

By using a mode superposition technique, the solution of equation (1) can be written as

$$w(\mathbf{x}, t) = \sum_{k=1}^{\infty} \Phi_k(\mathbf{x}) T_k(t), \tag{2}$$

where k is the mode number, $\Phi_k(\mathbf{x})$ are the mass normalized undamped mode shapes and $T_k(t)$ is the kth normal co-ordinate.

If the mode functions satisfy the following orthogonality relationships, then the modes can be uncoupled:

$$\int_S \bar{m}(\mathbf{x}) \Phi_h(\mathbf{x}) \Phi_k(\mathbf{x})\, d\mathbf{x} = \delta_{hk}, \qquad h,k = 1,2,3,\ldots,\infty,$$

$$\int_S L\{\Phi_h(\mathbf{x})\} \Phi_k(\mathbf{x})\, d\mathbf{x} = \omega_k^2 \delta_{hk}, \qquad h,k = 1,2,3,\ldots,\infty,$$

$$\int_S C\{\Phi_h(\mathbf{x})\} \Phi_k(\mathbf{x})\, d\mathbf{x} = 2\zeta_k \omega_k \delta_{hk}, \; h,k = 1,2,3,\ldots,\infty, \tag{3}$$

where δ_{hk} is equal to 1 if $h = k$ and zero otherwise, ω_k and ζ_k are the kth undamped natural frequency and modal damping ratio, respectively, and S is the surface area of the bridge. The first two orthogonality relationships are satisfied if the mode shapes are computed from the undamped free vibration corresponding to equation (1) ($f(\mathbf{x}, t) = 0$), while the third will be satisfied if (proportional damping)

$$C\left\{\frac{\partial w}{\partial t}(\mathbf{x}, t)\right\} = \alpha \bar{m}(\mathbf{x}) \frac{\partial w}{\partial t}(\mathbf{x}, t) + \beta L\left\{\frac{\partial w}{\partial t}(\mathbf{x}, t)\right\}, \tag{4}$$

α and β being arbitrary constants. In this case ζ_k is given by reference [29]:

$$2\zeta_k \omega_k = \alpha + \beta \omega_k^2. \tag{5}$$

Substituting the modal expansion (2) into equation (1), multiplying by $\Phi_k(\mathbf{x})$ and integrating over the surface of the bridge, one would obtain the response of the system for mode k:

$$\frac{\mathrm{d}^2 T_k}{\mathrm{d}t^2}(t) + 2\zeta_k \omega_k \frac{\mathrm{d}T_k}{\mathrm{d}t}(t) + \omega_k^2 T_k(t) = \int_S \Phi_k(\mathbf{x}) f(\mathbf{x}, t)\, \mathrm{d}\mathbf{x}, \quad k = 1,2,3, \ldots, \infty \quad (6)$$

The impulse response function related to each mode has the following form:

$$h_k(t) = \frac{\mathrm{e}^{-\zeta_k \omega_k t} \sin(\omega_k \sqrt{1-\zeta_k^2}\, t)}{\omega_k \sqrt{1-\zeta_k^2}}, \qquad t \geqslant 0,\ \zeta_k < 1. \quad (7)$$

It can be shown [7] that the response of the system to a set of dynamic wheel loads, $P_l(t)$, applied at moving position $\mathbf{x}_l(t)$ (see Figure 1) and assumed positive upwards, is given by the convolution integral:

$$w(\mathbf{x}, t) = \sum_{l=1}^{N_t} \sum_{k=1}^{\infty} \Phi_k(\mathbf{x}) \int_{-\infty}^{\infty} h_k(t-\tau) \Phi_k(\mathbf{x}_l(\tau)) P_l(\tau)\, \mathrm{d}\tau, \quad (8)$$

where N_t is the number of tyres of the vehicle. The convolution integral is evaluated in the time domain, but it is also possible to choose its frequency domain formulation by taking advantage of the fast Fourier transform algorithm [7].

2.2. THE BRIDGE MODEL: FLEXURAL VIBRATION OF RECTANGULAR PLATES

The bridge is modelled as a multi-span thin rectangular plate, of uniform thickness and isotropic material, lying in the x–y plane and bounded by the lines at $x = 0$, a and at $y = 0$, b (Figure 2). The N-span continuous plate is simply supported along the edges $x = 0$ and $x = a$, free at the edges $y = 0$ and $y = b$ and passes over N-1 rigid line supports.

The equation of motion for the free vibrations of lightly damped rectangular plates, according to reference [29], is

$$\bar{m} \frac{\partial^2 w}{\partial t^2} + C\left\{\frac{\partial w}{\partial t}\right\} + D\left(\frac{\partial^4 w}{\partial x^4} + 2\frac{\partial^4 w}{\partial x^2 \partial y^2} + \frac{\partial^4 w}{\partial y^4}\right) = 0, \quad (9)$$

where $D = Eh^3/12(1-\nu^2)$ is the plate flexural stiffness, E is the Young's modulus, h is the plate thickness, ν is the Poisson's ratio. The approximate solutions for frequencies and mode shapes of the vibrating plate are obtained by using the Rayleigh–Ritz method, which consists of assuming the undamped deflection function as a series of admissible functions with coefficients minimizing Rayleigh's quotient. For a uniform plate, vibrating harmonically with amplitude $\Phi(x, y)$ and

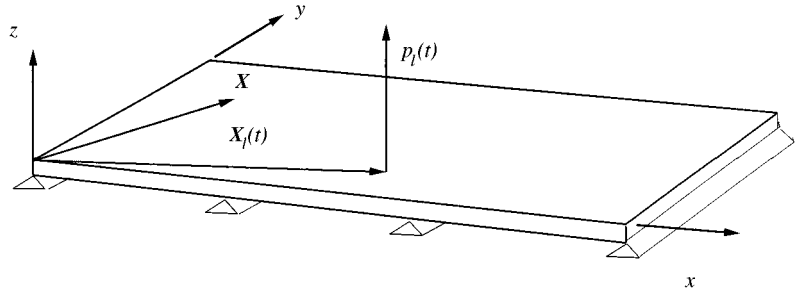

Figure 1. Continuous model of the bridge.

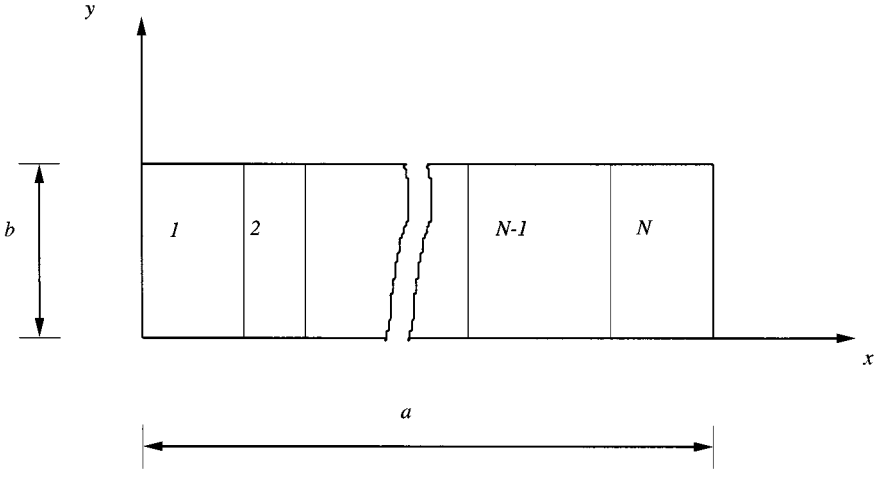

Figure 2. N-span continuous rectangular plate.

angular frequency ω, the maxima strain and kinetic energies are given by:

$$V_{\max} = \frac{D}{2}\int_S \left[\left(\frac{\partial^2 \Phi}{\partial x^2}\right)^2 + \left(\frac{\partial^2 \Phi}{\partial y^2}\right)^2 + 2\nu\,\frac{\partial^2 \Phi}{\partial x^2}\,\frac{\partial^2 \Phi}{\partial y^2} + 2(1-\nu)\left(\frac{\partial^2 \Phi}{\partial x \partial y}\right)^2\right] \mathrm{d}x\mathrm{d}y, \quad (10)$$

$$T_{\max} = \frac{1}{2}\,\bar{m}\omega^2 \int_S \Phi^2(x, y)\mathrm{d}x\mathrm{d}y. \quad (11)$$

It is now opportune to introduce the undimensioned space variables $\xi = x/a$ and $\eta = y/b$.

Hence the deflection shape Φ becomes

$$\Phi(\xi, \eta) = \sum_i \sum_j A_{ij}\varphi_i(\xi)\psi_j(\eta), \quad (12)$$

where $\varphi_i(\xi)$ and $\psi_j(\eta)$ are the assumed admissible functions along the x and y directions, while A_{ij} are the undetermined coefficients. According to the procedure adopted in references [13, 23], $\varphi_i(\xi)$ and $\psi_j(\eta)$ are eigenfunctions satisfying the equation of motion for free vibrations of an Euler–Bernoulli beam, in the x and y directions respectively, and also the desired boundary conditions on both the perimeter and the rigid line supports. In particular $\varphi_i(\xi)$ are the eigenfunction of an Euler–Bernoulli beam on multiple supports.

Substituting equation (12) into equations (10) and (11) and minimizing Rayleigh's quotient with respect to each coefficient A_{ij} leads to the eigenvalue equation

$$\sum_m \sum_n [C_{mnij} - \lambda B_{mnij}] A_{mn} = 0,\ i,j = 1,2,3,\ \ldots\ , \tag{13}$$

where

$$\lambda = \frac{\bar{m}\omega^2 a^4}{D},$$

$$C_{mnij} = E_{mi}^{(22)} F_{nj}^{(00)} + \left(\frac{a}{b}\right)^4 E_{mi}^{(00)} F_{nj}^{(22)} + \nu\left(\frac{a}{b}\right)^2 (E_{mi}^{(02)} F_{nj}^{(20)} + E_{mi}^{(20)} F_{nj}^{(02)})$$

$$+ 2(1-\nu)\left(\frac{a}{b}\right)^2 E_{mi}^{(11)} F_{nj}^{(11)},\ B_{mnij} = E_{mi}^{(00)} F_{nj}^{(00)},$$

$$E_{mi}^{(rs)} = \int_0^1 \frac{\mathrm{d}^r \varphi_m}{\mathrm{d}\xi^r} \frac{\mathrm{d}^s \varphi_i}{\mathrm{d}\xi^s}\, \mathrm{d}\xi, \qquad F_{nj}^{(rs)} = \int_0^1 \frac{\mathrm{d}^r \psi_n}{\mathrm{d}\eta^r} \frac{\mathrm{d}^s \psi_j}{\mathrm{d}\eta^s}\, \mathrm{d}\eta. \tag{14}$$

2.3. VEHICLE MODEL AND DYNAMIC BRIDGE–VEHICLE INTERACTION

Figure 3 shows a diagram of the vehicle dynamic model excited by bridge surface irregularities. The vehicle body is rigid, subject to heave, roll and pitch motions. The linear vehicle model, similar to that employed in reference [30] and also similar to that described in reference [27], which were modelled according to the truck design loadings included in the American Association of State High-way and Transportation Officials (AASHTO) specifications, has some limitations since flexible body modes, wheel unbalance, transverse motions of the centre of gravity, suspensions kinematics, gyroscopic effects, etc., have all been left aside. The seven second order ordinary differential equations have been obtained by using Lagrange's formulation and they have been gathered into 14 first order state equations.

The displacements under the tyres $u_{1l}, u_{1r}, u_{2l}, u_{2r}$, representing the forcing terms in the vehicle's equations of motion, are given by the sum of the surface irregularities $r(t)$ and of the bridge deflection $w(\mathbf{x}_l, \mathrm{t})$, corresponding to the tyre position $\mathbf{x}_l$ at

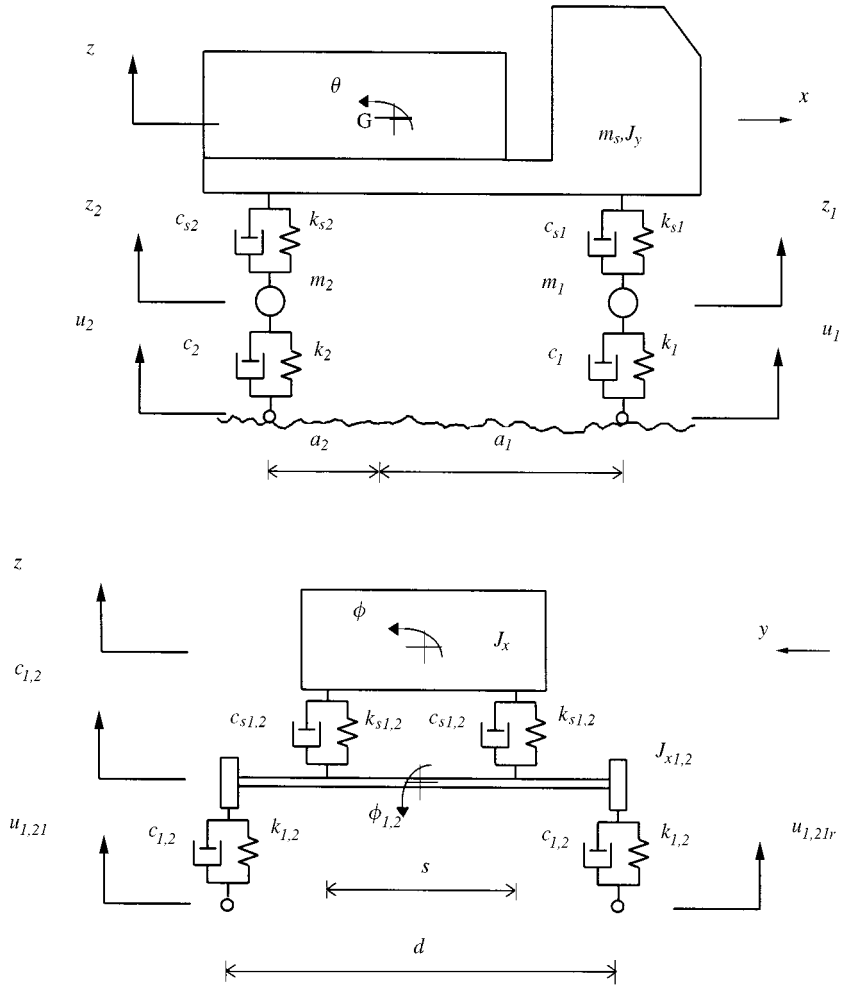

Figure 3. Sketch of the seven d.o.f. system and its parameters. z, z_1, z_2 = vertical displacement of body, front and rear axle; θ = pitch displacement of the body; ϕ = roll displacement of the body; ϕ_1, ϕ_2 = front and rear axle angular displacements; u_{1l}, u_{1r}, u_{2l}, u_{2r} = road displacements under left front, right front, left rear, right rear tyre.

time t, that is,

$$u(t) = w(\mathbf{x}_l, t) + r(t). \tag{15}$$

The loads $P_l(t)$ transmitted by the moving tyres to the bridge surface are therefore functions of the bridge deflection $w(\mathbf{x}_l, t)$: the determination of the bridge dynamic response involves an integral equation and therefore requires the iterative procedure presented in reference [7] and illustrated in the flow-chart of Figure 4, where T_{vp} represents the time the vehicle takes to cross the bridge completely and *tol* is the convergence tolerance. A similar iterative method, called the "iterative dynamic substructuring method (IDSM)" can be found in reference [31]. The fourteen first

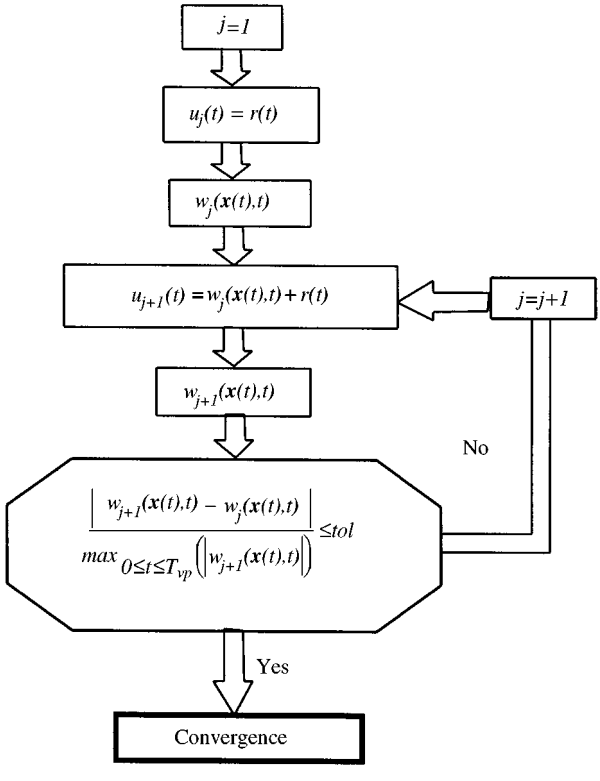

Figure 4. Iterative procedure for the determination of bridge deflection.

order state equations of the vehicle have been solved by Runge-Kutta numerical integration.

2.4. MODEL OF THE BRIDGE SURFACE IRREGULARITIES

In references [6, 9] it is shown how an easy and realistic description of the road surface roughness can be given through an ergodic stationary Gaussian random process, described by its spectral density S versus the spatial frequency γ:

$$S(\gamma) = \begin{cases} a \cdot \gamma^{-\beta}, & \gamma_0 < \gamma < \gamma_J, \\ 0 & \gamma < \gamma_0; \gamma > \gamma_J, \end{cases} \tag{16}$$

where γ_0 and γ_J are cut-off spatial frequencies, β is a constant, whose value is 2, and a is a spectral roughness coefficient, whose value depends on the road conditions: $a < 0{\cdot}4 \times 10^{-6}$ m/cycle for a good surface, $0{\cdot}4 \times 10^{-6} < a < 0{\cdot}64 \times 10^{-6}$ m/cycle for an ordinary surface and $0{\cdot}64 \times 10^{-6} < a < 1 \times 10^{-6}$ m/cycle for a damaged surface. If V (m/s) is the constant speed of the vehicle, the temporal frequency f (Hz) corresponding to the spatial frequency γ, is

$$f = \gamma V. \tag{17}$$

So, road irregularity exciting the vehicle at time t in the position $x(t) = Vt$ along the bridge span can be obtained according to the procedure adopted by reference [8].

In order to generate the appropriate correlation between the tracks roughness under the left and right wheels, the hypothesis of isotropy of the road surface is adopted here. It can be shown through a comparison between the measured and calculated coherency of two parallel tracks [32, 33] that the proposed model is applicable in a variety of cases. The two- dimensional power spectral density of the road surface satisfying the hypothesis of isotropy (invariance with respect to any rotation of the reference co-ordinate system) has the following form, as reported in reference [32]:

$$F(\gamma_x, \gamma_y) = \frac{a}{2(\gamma_x^2 + \gamma_y^2)^{3/2}}, \tag{18}$$

where γ_x and γ_y are the spatial frequencies along the x- and y- axis. The coherency function between left and right tracks thus becomes

$$\chi(\gamma_x) = \frac{|S_{lr}(\gamma_x)|}{S(\gamma_x)} = \int_0^{+\infty} \frac{\cos(2\pi\lambda\gamma_x d)}{(1 + \lambda^2)^{3/2}} \, \mathrm{d}\lambda, \tag{19}$$

where d is the trackwidth, $S_{lr}(\gamma_x)$ is the cross-spectral density of the two profiles and $\lambda = \gamma_y/\gamma_x$. This coherency function can be easily computed by means of the FFT algorithm, giving curves identical to those presented in reference [33], obtained using a different methodology. The coherency function, plotted versus the dimensionless variable $\gamma_x d$, computed from equation (19), is reported in Figure 5.

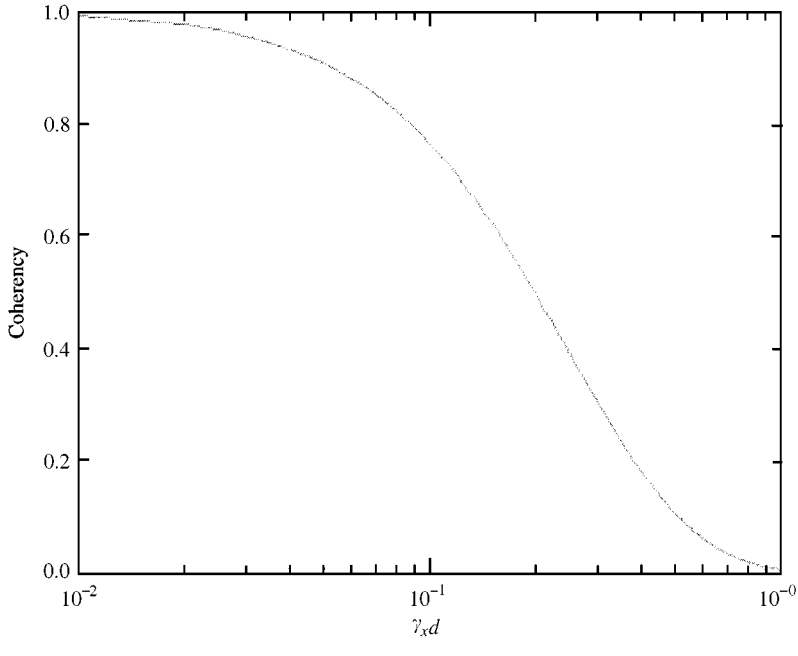

Figure 5. Isotropic coherency function versus γ_xd.

3. NUMERICAL EXAMPLES

3.1. BRIDGE AND VEHICLE MODEL PROPERTIES

A three-span continuous bridge has been analysed with the following geometry and material properties (see Figure 6):

$$l_1 = l_2 = l_3 = 26.4\ \text{m}, \quad b = 10.7\ \text{m}, \quad h = 0.95\ \text{m}, \quad E = 14.54 \times 10^{10}\ \text{N/m}^2,$$

$$\nu = 0.3, \ \bar{m} = 2375\ \text{kg/m}^2.$$

In order to compare the theoretical modal properties, three simple models for the bridge have been developed. In the first model, the bridge has been approximated by an Euler–Bernoulli beam on rigid supports, in the second a plate has been adopted, using the method described in Section 2.2, while in the third a finite-element (FE) analysis has been carried out. The finite-element model consists of 2400 (800 in each span) elements equally spaced along the three directions. The chosen elements are eight-noded linear bricks, whose number has been set on the basis of convergency tests performed on the resulting modal properties of the structure. In particular, in order to also respect the restrictions imposed on the element aspect ratios by the FE code, four subdivisions along the z direction, 10 along the y (transverse) direction and 60 along the x (longitudinal) direction were used. Obviously, since the beam theory cannot predict the torsional modes of the bridge, a plate model is necessary for a full comparison with the FE model. The frequencies of the plate model have been obtained by using the Rayleigh–Ritz method with 9×5 and 17×9 terms in the series (12), while the modal damping ratio has been assumed to be equal to 0.02 for the first two modes, and for the remaining modes it has been chosen so that the orthogonality conditions (3) could be satisfied. The bridge modal parameters are summarized in Table 1 and the mode shapes in Figure 7.

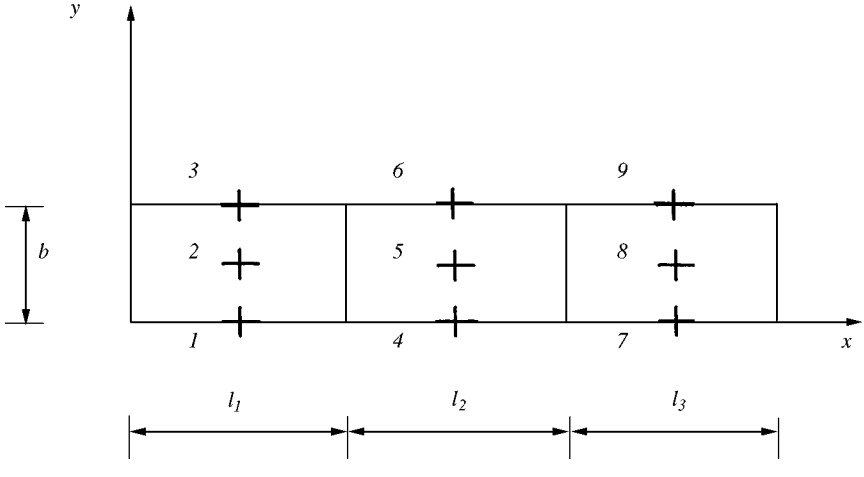

Figure 6. Bridge geometry and computed deflection points.

TABLE 1
Bridge modal parameters

Mode	Beam model frequency (Hz)	Plate model frequency (Hz) No of terms in series (12)		Damping ratio Ratio ζ_k	FE model frequency frequency (Hz)
		$i \times j = 9 \times 5$	$i \times j = 17 \times 9$		
1	4·71	4·79	4·77	0·0200	4·75
2	6·04	6·19	6·17	0·0200	6·13
3	8·82	9·11	9·09	0·0225	9·02
4	–	16.65	16·65	0·0337	16·19
5	–	17.55	17·53	0·0351	16·98
6	18·86	19·37	19·31	0·0381	18·90
7	–	19·57	19·51	0·0384	19·28
8	21·49	22·16	22·10	0·0428	22·03

TABLE 2
Vehicle modal parameters

	Mode	Natural frequency (Hz)	Damping ratio ζ_v
1	Body roll	0·95	0·33
2	Body pitch	1·06	0·59
3	Body heave	1·19	0·28
4	Front axle bounce	7·69	0·87
5	Front axle roll	8·90	0·41
6	Rear axle bounce	9·54	0·60
7	Rear axle roll	12·32	0·38

In this study, the seven d.o.f. vehicle model presented in Figure 3 has been chosen. The characteristics of the selected vehicle are shown in Appendix A, while its modal parameters are summarized in Table 2.

3.2. NUMERICAL SIMULATIONS AND RESULTS

The results reported hereafter have been obtained considering crossing speeds in the range 10–45 m/s; the road has been considered both perfectly smooth (results in Figures 8–12) and rough (results in Figures 13–16).

The bridge response has been computed by superimposing the first 13 modes up to 43.89 Hz, thus reaching a good compromise between computational time and accuracy of results. For the latter reason, and considering Table 1 and Figure 7, the modes have been calculated by using the Rayleigh–Ritz method with 9×5 terms in the series (12).

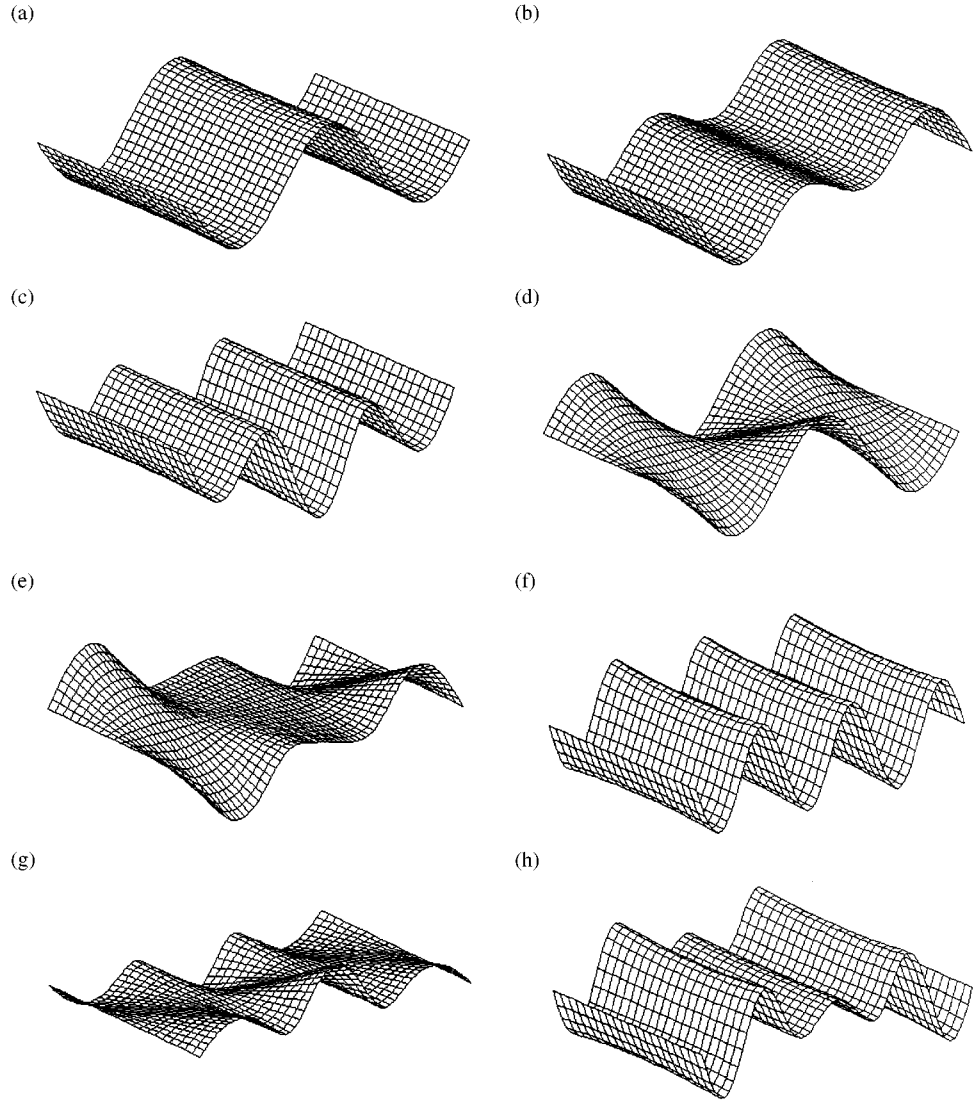

Figure 7. First eight modes of the bridge. Modes: (a) 1, $f = 4.79$ Hz; (b) 2, $f = 6.19$ Hz; (c) 3, $f = 9.11$ Hz; (d) 4, $f = 16.65$ Hz; (e) 5, $f = 17.55$ Hz; (f) 6, $f = 19.37$ Hz; (g) 7, $f = 19.57$ Hz; (h) 8, $f = 22.16$ Hz.

The vehicle crosses the bridge along the positive x direction with its right tyres at a distance of 1 m from the right border of the bridge. Attention was focused on mid-span points, and in particular on points 1–9 in Figure 6.

The Amplification Factor is defined as the ratio of the maximum dynamic deflection to the maximum static deflection ($V = 0$) [6]. Very irregular behaviour, possibly superimposed on an almost linear trend, can be easily noticed by looking at Figures 8–10. It is considered that this is due to the damped oscillation of each mode contributing to the total deflection of the bridge.

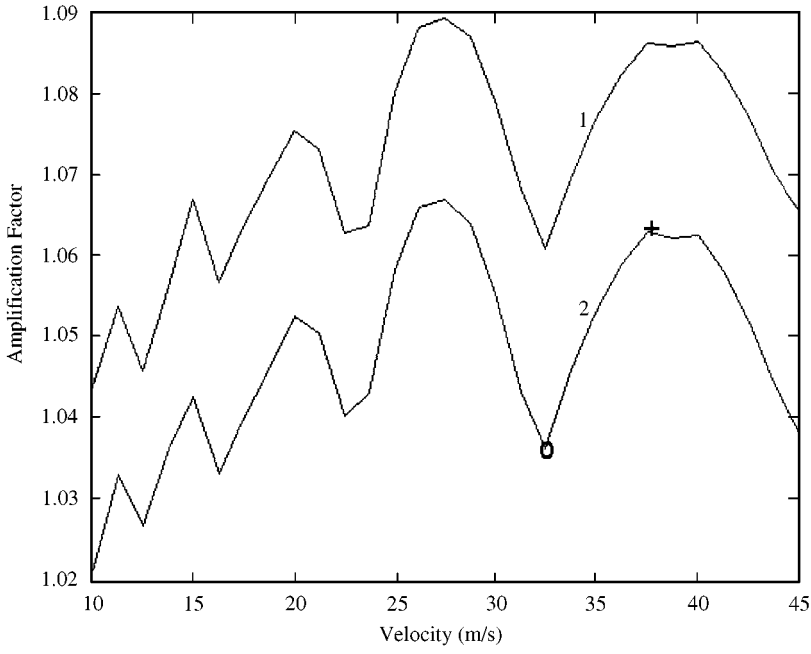

Figure 8. Amplification Factor versus vehicle speed for points 1 and 2.

Figure 11 explains why the values of the Amplification Factor marked with "**O**" and " + " in Figure 8 are quite different, despite the slight velocity difference ($V = 32.5$ and 37.5 m/s). The reason is the different relative phase of the mode contributions as shown in Figure 11 (c–d); in particular, the contribution of the first and second modes, the most important for the total oscillation of point 2 (Figure 6), is highlighted in the zoomed frame. The modes over the fifth give a negligible contribution.

Figure 12, referring to point 1, highlights the relevant contribution of the torsional mode shapes [Figure 7(d–e)] to bridge deflection, often neglected in previous publications; obviously all the points in the centreline of the bridge do not undergo any torsional effects.

An example of the tracks used in the numerical simulations in the case of the rough road surface is reported in Figure 13. The left line is generated according to the procedure adopted by reference [8], while the right line has been obtained by a trial-and-error procedure in order to reproduce a coherency function of the kind plotted in Figure 5 for a given value of d (see Appendix A). By comparing Figures 5 and 14, relative to the tracks shown in Figure 13, it can be seen that, with an appropriate spatial frequency shift, the agreement in the range of interest is satisfactory; real data reported in the literature [32, 33] also show a similar level of agreement.

Figure 15 shows the great sensibility of the Amplification Factor with respect to the damping of the vehicle suspensions and to the roughness of the road

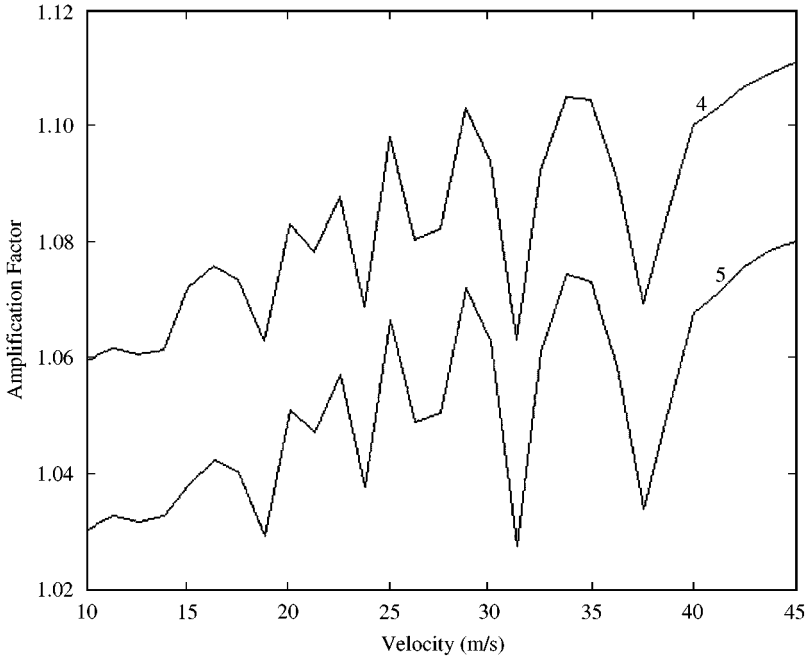

Figure 9. Amplification Factor versus vehicle speed for points 4 and 5.

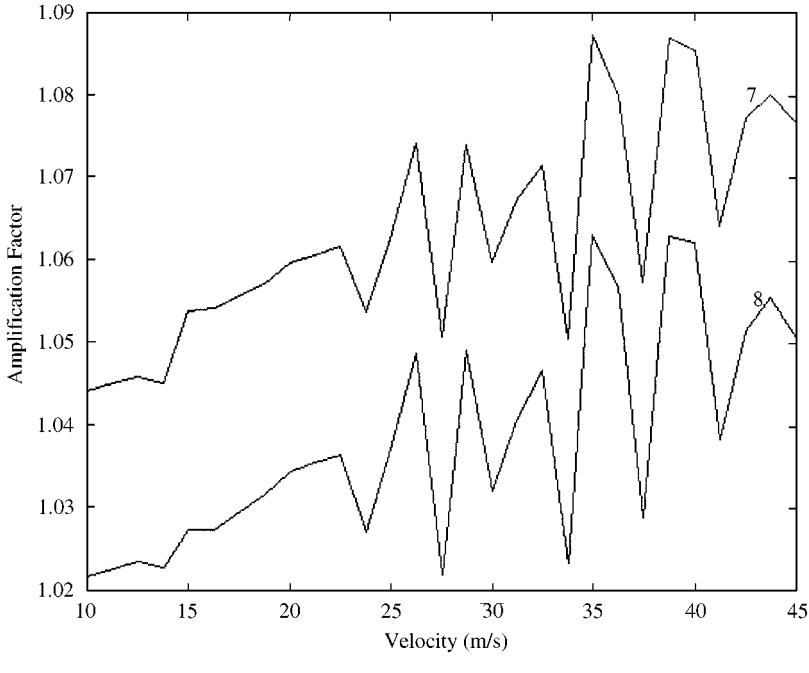

Figure 10. Amplification Factor versus vehicle speed for points 7 and 8.

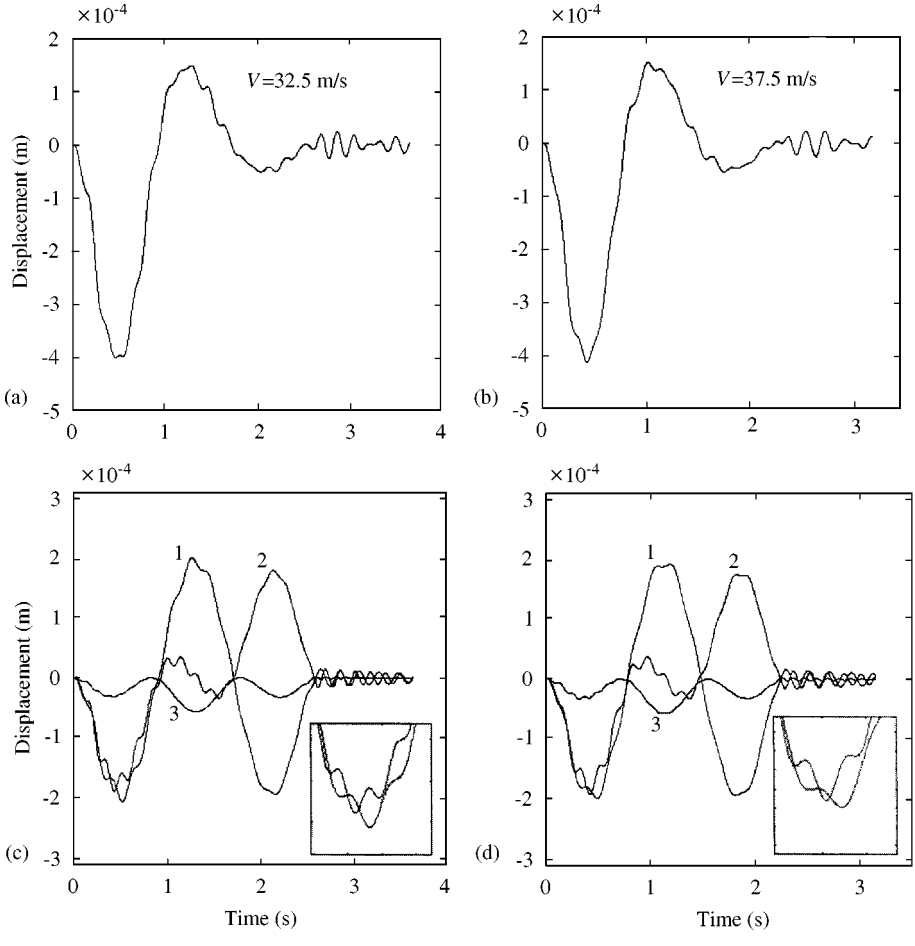

Figure 11. Time histories relative to deflections in point 2 for two different speeds. (a) and (c) correspond to the point marked by "**O**" in Figure 8; (b) and (d) correspond to the point marked by " + " in the same figure. In figure (c) and (d) the mode contributions are highlighted.

(i.e. maximum Amplification Factors are reached for low vehicle damping and for the damaged surface as classified in Section 2.4).

In order to give a statistical significance to the results, 20 random profiles, satisfying the hypothesis of isotropy, have been generated and, for each profile, 29 numerical simulations at different velocities have been performed. In Figures 16(a,b) the variation of the minimum, mean and maximum values of the Amplification Factor and the ratio of the standard deviation to the mean value (lower than 5%) versus the velocity, relative to point 5, are plotted. By way of comment to Figure 16, the randomness of the results, due to the interaction of two main different factors, i.e. the surface roughness and the vehicle damping, should be pointed out. From this point of view, one should also remember that in some cases the maximum values can definitely be higher (see for example Figure 15).

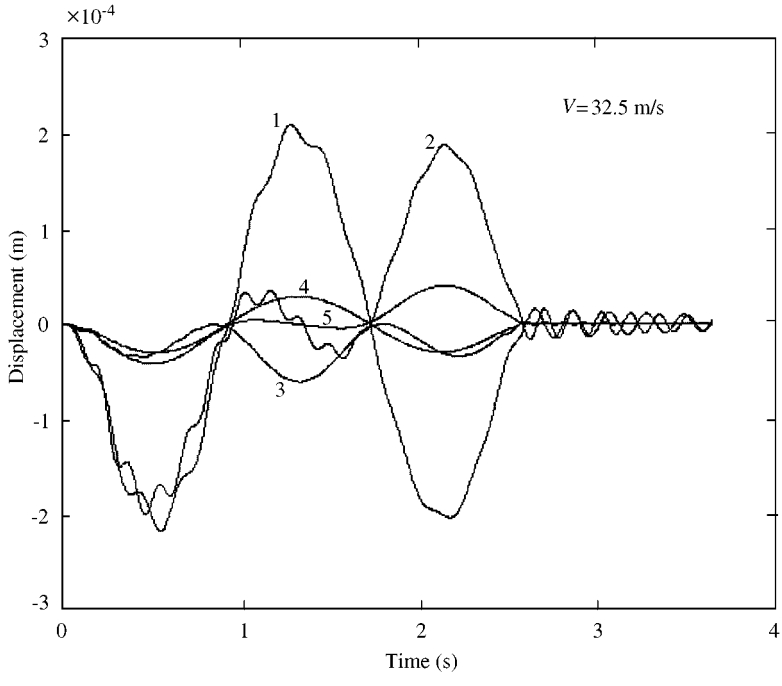

Figure 12. Mode contributions to total deflection in point 1.

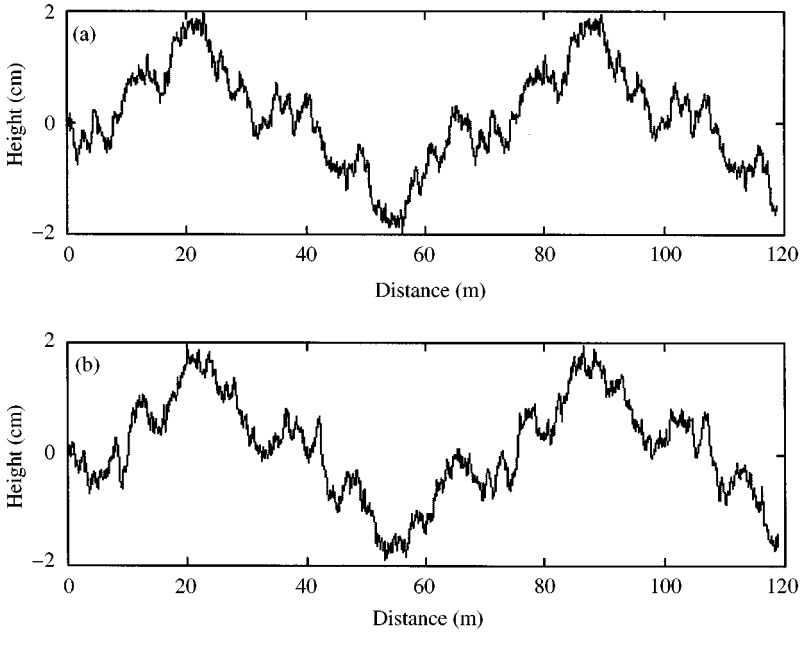

Figure 13. Vertical surface profiles of a damaged road: (a) left line; (b) right line. The lower and upper cut-off spatial frequencies are $\gamma_0 = 0.015$ cycles/m and $\gamma_J = 10$ cycles/m, respectively.

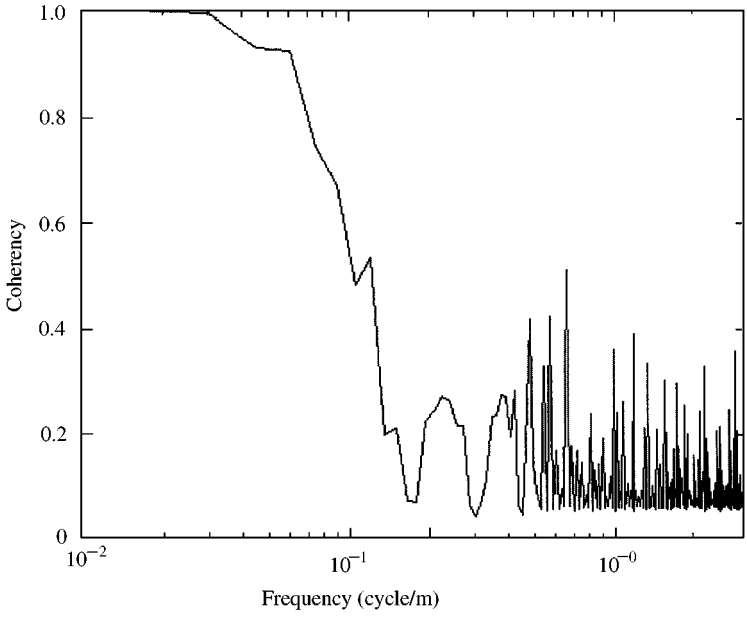

Figure 14. Generated coherency function versus spatial frequency for $d = 2.05$ m.

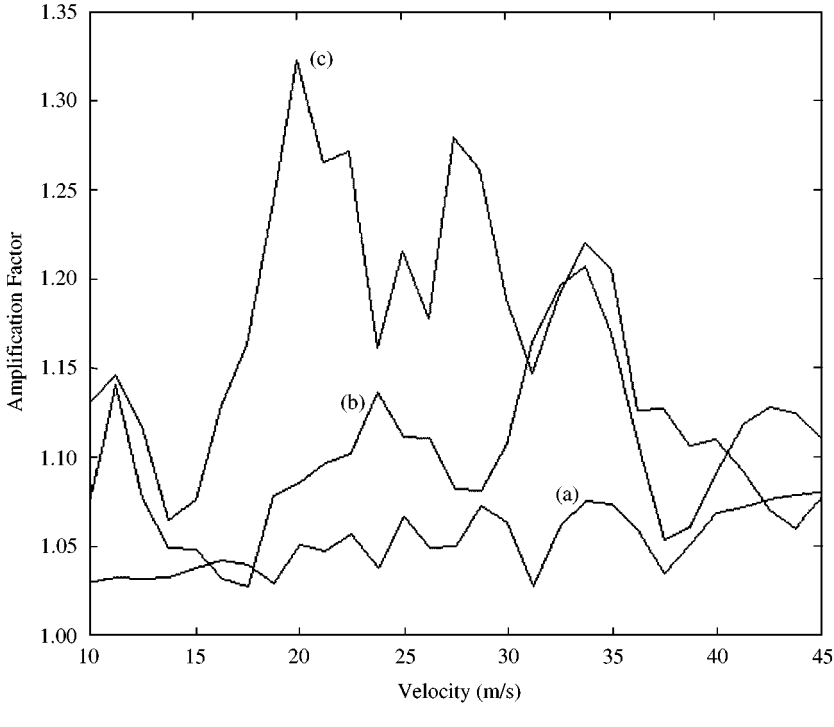

Figure 15. Amplification Factor relative to point 5 versus vehicle speed for a smooth (a) and rough (b) surface (Figure 13). The curve (c) refers to a rough surface and to very small values of suspension damping (the damping matrix of the vehicle–system is reduced to one-tenth of the original).

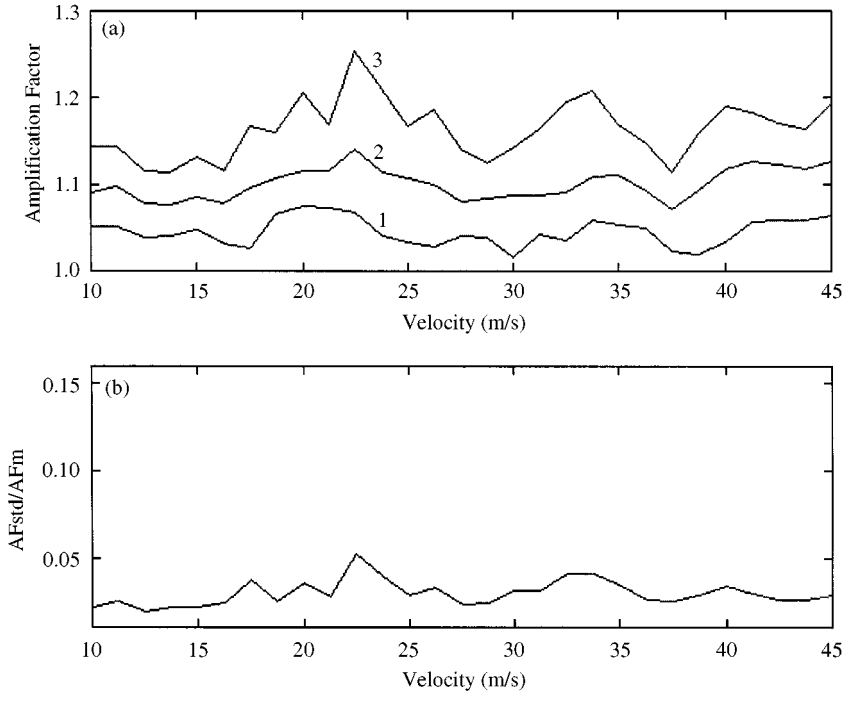

Figure 16. Variation with the velocity of the minimum (1), mean (2) and maximum (3) values of the Amplification Factor for point 5 (a) and of the ratio of the standard deviation (AFstd) to the mean value (AFm) (b).

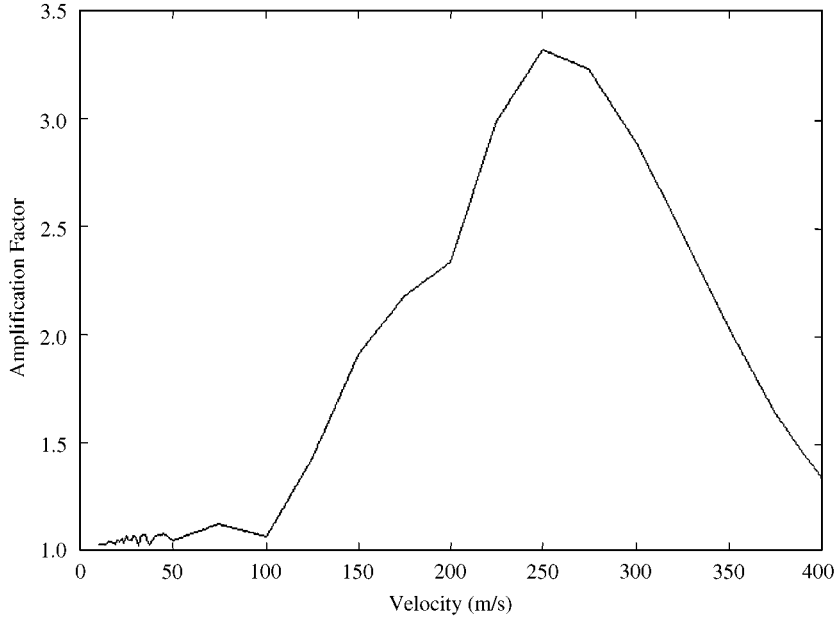

Figure 17. Amplification Factor versus load speed for points 5 (smooth surface).

It is possible to find many definitions for the speed parameter in the literature and the following has been chosen [27]:

$$\sigma = V/2lf_1, \tag{20}$$

where l is the length of any single span and f_1 is the frequency of the first mode of the bridge. Figure 17 represents the variation of the Amplification Factor at point 5 for a smooth surface as a function of the vehicle speed. The graph explains how the Amplification Factor changes within the speed range considered. It is clear that the maximum reached by the Amplification Factor at $V = 252.9$ m/s [corresponding to $\sigma = 1$ in equation (20)] is well above any sensible vehicle speed.

4. CONCLUSIONS AND FUTURE WORK

In this paper the dynamic interaction between a moving vehicle, modelled as a seven d.o.f. spatial system, and a bridge, modelled as a multi-span plate, has been studied.

The numerical examples reported are relative to a three span bridge. The theoretical modes, defined by means of the Rayleigh–Ritz approach, have been found to be in good agreement with an FE model thus giving confidence to the analytical results.

The technique discussed and implemented includes both the flexural and torsional modes of the structure, the roughness of the road and, in principle, allows the introduction of any model of vehicle.

The good results obtained gave rise to the authors' curiosity and future work should include: the problem of interaction in presence of orthotropic plates, the line support stiffnesses, more sophisticated models of the bridge, including shear deformation and rotary inertia effects as in reference [34], curved or skew bridges [35–37], the simultaneous presence of more than one vehicle on the bridge, more sophisticated models of the roughness of the road, the influence of vehicle characteristics, and perhaps, comparison with the actual results of a real structure.

REFERENCES

1. S. Timoshenko, D. H. Young and W. Weaver 1974 *Vibration Problems in Engineering*. New York: Wiley, fourth edition.
2. L. Fryba 1972 *Vibration of Solids and Structures under Moving Loads*. Groningen: Noordoff.
3. G. Michaltsos, D. Sophianopoulos and A. N. Kounadis 1996 *Journal of Sound and Vibration* **191**, 357–362. The effect of a moving mass and other parameters on the dynamic response of a simply supported beam.
4. R. H. Gutierrez and P. A. A. Laura 1996 *Journal of Sound and Vibration* **195**, 353–358. Transverse vibrations of beams traversed by point masses: a general, approximate solution.
5. H. P. Lee 1996 *Journal of Sound and Vibration* **198**, 249–256. The dynamic response of a Timoshenko beam subjected to a moving mass.
6. R. K. Chatterjee, T. K. Datta and C. S. Surana 1994 *Journal of Sound and Vibration* **169**, 619–632. Vibration of continuous bridges under moving vehicles.

7. M. F. Green and D. Cebon 1994 *Journal of Sound and Vibration* **170**, 51–78. Dynamic response of highway bridges to heavy vehicle loads: theory and experimental validation.
8. E. S. Hwang and A. S. Nowak 1991 *American Society of Civil Engineers, Journal of Structural Engineering* **117**, 1413–1434. Simulation of dynamic load for bridges.
9. O. Coussy, M. Said and J. P. Van hoove 1989 *Journal of Sound and Vibration* **130**, 313–320. The influence of random surface irregularities on the dynamic response of bridges under suspended moving loads.
10. J. E. Snyder and D. N. Wormley 1977 *American Society of Mechanical Engineers, Journal of Dynamic Systems, Measurements, and Control* **99**, 23–33. Dynamic interactions between vehicles and elevated, flexible randomly irregular guideways.
11. H. S. Zibdeh and R. Rackwitz 1995 *Journal of Sound and Vibration* **188**, 479-495. Response moments of an elastic beam subjected to Poissonian moving loads.
12. H. S. Zibdeh and R. Rackwitz 1996 *Journal of Sound and Vibration* **195**, 85–102. Moving loads on beams with general boundary conditions.
13. A. W. Leissa 1973 *Journal of Sound and Vibration* **31**, 257–293. The free vibration of rectangular plates.
14. T. Sakata 1976 *Journal of Sound and Vibration* **47**, 577–583. Eigenvalues of orthotropic continuous plates with two opposite sides simply supported.
15. D. J. Gorman 1982 *Free Vibration Analysis of Rectangular Plates.* New York: Elsevier North Holland.
16. C. S. Kim, P. G. Young and S. M. Dickinson 1990 *Journal of Sound and Vibration* **143**, 379–394. On the flexural vibration of rectangular plates approached by using simple polynomials in the Rayleigh-Ritz method.
17. K. M. Liew and K. Y. Lam 1991 *Journal of Sound and Vibration* **147**, 255–264. Vibration analysis of multi-span plates having orthogonal straight edges.
18. R. B. Bhat 1991 *Journal of Sound and Vibration* **149**, 170–172. Vibration of rectangular plates on point and line supports using characteristic orthogonal polynomials in the Rayleigh-Ritz method.
19. G. N. Geannakakes 1995 *Journal of Sound and Vibration* **182**, 441–478. Natural frequencies of arbitrarily shaped plates using the Rayleigh-Ritz method together with natural co-ordinate regions and normalized characteristic orthogonal polynomials.
20. R. B. Bhat, P. A. A. Laura, R. G. Gutierrez, V. H. Cortinez and H. C. Sanzi 1990 Journal of Sound and Vibration **138**, 205–219. Numerical experiments on the determination of natural frequencies of transverse vibrations of rectangular plates of non-uniform thickness.
21. G. B. Warburton 1976 *Journal of Sound and Vibration* **45**, 461–466. Comment on "A note on forced vibrations of a clamped rectangular plate".
22. K. M. Liew, K. C. Hung and M. K. Lim 1995 *Journal of Sound and Vibration* **182**, 709–727. Three-dimensional vibration of rectangular plates: effect of thickness and edge constraints.
23. D. Young 1950 *Journal of Applied Mechanics* **17**, 448–453. Vibration of rectangular plates by the Ritz method.
24. R. B. Bhat 1985 *Journal of Sound and Vibration* **102**, 493–499. Natural frequencies of rectangular plates using characteristic orthogonal polynomials in the Rayleigh-Ritz method.
25. K. M. Liew, K. Y. Lam and S. T. Chow 1990 *Computers and Structures* **34**, 79–85. Free vibration analysis of rectangular plates using orthogonal plate function.
26. R. Jones and B. J. Milne 1976 *Journal of Sound and Vibration* **45**, 309–316. Application of the extended Kantorovich method to the vibration of clamped rectangular plates.
27. T. L. Wang, D. Huang and M. Shahawy 1992 *American Society of Civil Engineers, Journal of Structural Engineering* **118**, 2222–2238. Dynamic response of multigirder bridges.

28. R. K. Gupta 1980 *American Society of Civil Engineers, Journal of the Engineering Mechanics Division* **106**, 377–394. Dynamic loading of highway bridges.
29. D. E. Newland 1989 *Mechanical Vibration Analysis and Computation*. Harlow: Longman.
30. A. J. Healey, E. Nathman and C. C. Smith 1977 *American Society of Mechanical Engineers, Journal of Dynamic Systems, Measurements, and Control* **99**, 284–292. An analytical and experimental study of automobile dynamics with random roadway inputs.
31. H. Hawk and A. Ghali 1981 *Canadian Journal of Civil Engineering* **8**, 392-401. Dynamic response of bridges to multiple truck loading.
32. E. Pellegrino and U. Tornar 1989 *7th International Modal Analysis Conference, Las Vegas, Nevada*, 867–873. A mathematical model of road excitation and its interaction with a non linear model of a car.
33. K. M. A. Kamash and J. D. Robson 1978 *Journal of Sound and Vibration* **57**, 89-100. The application of isotropy in road surface modeling.
34. K. M. Liew, Y. Xiang and S. Kitipornchai 1993 *Computers and Structures* **49**, 1–78. Transverse vibration of thick rectangular plates I, II, III, IV.
35. C. S. Huang, A. W. Leissa and O. G. McGee 1993 *Journal of Applied Mechanics* **60**, 478–483. Exact analytical solutions for the vibrations of sectorial plates with simply supported radial edges.
36. K. M. Liew and K. Y. Lam 1993 *International Journal of Mechanical Sciences* **35**, 129–139. On the use of 2D orthogonal polynomials in the Rayleigh-Ritz method for flexural vibration of annular sector plates of arbitrary shape.
37. K. M. Liew and C. M. Wang 1993 *Computers and Structures* **49**, 941–951. Vibration studies on skew plates: treatment of internal line supports.

APPENDIX A: VEHICLE CHARACTERISTICS

The characteristics of the selected seven d.o.f.s vehicle (see Figure 3) are

$a_1 = 3.153$ m, $a_2 = 1.577$ m, $d = 2.05$ m, $s = 1.41$ m;

$m_s = 17000$ kg, $m_1 = 600$ kg, $m_2 = 1000$ kg, $J_y = 90 \times 10^3$ kg m^2, $J_{x1} = 550$ kg m^2, $J_{x2} = 600$ kg m^2, $J_x = 13\,000$ kg m^2;

$k_1 = 785 \times 10^3$ N/m, $k_2 = 1.57 \times 10^6$ N/m, $k_{s1} = 116 \times 10^3$ N/m, $k_{s2} = 373 \times 10^3$ N/m;

$c_1 = 1 \times 10^2$ N s/m, $c_2 = 2 \times 10^2$ N s/m, $c_{s1} = 25 \times 10^3$ N s/m, $c_{s2} = 35 \times 10^3$ N s/m.